Jpn. J. Appl. Phys. Vol. 41 (2002) pp. 4878–4882
Part 1, No. 7B, July 2002

Review Paper

First and Second-Order Resonance Raman Process in Graphite and Single Wall Carbon Nanotubes

Riichiro SAITO, Ado JORIO[1,2], Antonio G. Souza FILHO[2,5], Gene DRESSELHAUS[3], Mildred S. DRESSELHAUS[2,4], Alexander GRÜNEIS, Luiz G. CANÇADO[1], Marcos A. PIMENTA[1]

Department of Electronic Engineering, University of Electro-Communications, Chofu, 182-8585 Tokyo, Japan
[1]*Departamento de Física, Universidade de Federal de Minas Gerais, Belo Horizonte-MG, 30123-970, Brazil*
[2]*Department of Physics, Massachusetts Institute of Technology, Cambridge, MA 02139-4307, USA*
[3]*Francis Bitter Magnet Laboratory, Massachusetts Institute of Technology, Cambridge, MA 02139-4307, USA*
[4]*Department of Electrical Engineering and Computer Science, Massachusetts Institute of Technology, Cambridge, MA 02139-4307, USA*
[5]*Departamento de Física, Universidade Federal do Ceará, Fortaleza-CE, 60455-760, Brazil*

(Received January 15, 2002; accepted for publication February 25, 2002)

Resonant Raman scattering for one single wall carbon nanotube spectroscopy is overviewed. First-order resonance Raman spectra of the radial breathing mode of *one* carbon nanotube is of importance for assigning (n, m) values to the nanotube. This assignment of (n, m) values is confirmed by the chirality dependence of other phonon modes. Second-order, one-phonon emission, and the inter-valley scattering processes of two dimensional graphite and of single wall carbon nanotubes are relevant to disorder-induced D-band Raman spectra. The dispersive nature of the D-band Raman spectra is explained by double resonance processes. Many weak Raman spectra appearing in the intermediate frequency range, which have been observed for a long time but never assigned so far, have recently been assigned as double resonance Raman peaks. The second-order Raman phonon frequencies can be used as a new fundamental tool for determining the phonon energy dispersion relations, especially for disordered materials and for zone boundary phonons. [DOI: 10.1143/JJAP.41.4878]

KEYWORDS: carbon nanotubes, Raman spectroscopy, graphite, D-band, double resonance theory

1. Introduction

Recently, we have succeeded in observing resonance Raman spectra from one single wall carbon nanotube (SWNT) grown by a chemical vapor deposition (CVD) method on a Si/SiO_2 surface.[1–4] The Raman spectra, thus obtained, have much smaller line widths ($\sim$5–10 cm^{-1}) than those obtained for SWNT bundles, which enables us to assign (n, m) values to a SWNT from its radial breathing mode (RBM) frequency by the use of theory.[5] The assignment of (n, m) is confirmed by other features in the Raman spectra of the same nanotube.[6–8] In this paper we first review the background of first- and second-order resonance Raman spectroscopy for a single carbon nanotube and then present new considerations for the dispersive Raman modes for individual single wall carbon nanotubes.

Important key factors for obtaining a Raman signal from a single nanotube are that: (1) a one-dimensional van Hove singularity in the joint-density of states (JDOS) of a SWNT which gives a sharp optical absorption at the corresponding energy, and that (2) the resonance condition with the incident or scattered photon is rigorously satisfied.[9] In one-dimensional materials, the van Hove singularities of the JDOS appear at the initial and final energy for a valence to conduction band transition denoted by E_{ii} for a pair of symmetrical energy subbands, and each singularity is proportional to $1/\sqrt{E - E_{ii}}$ for $E \geq E_{ii}$. A very sharp peak in the JDOS around $E = E_{ii}$ can be treated as a discrete molecular level. A rigorous resonance corresponds to the case when the laser excitation energy E_{laser} exactly matches the electronic absorption transition, thereby providing a strong contribution to the Raman intensity that is mainly associated with the singularities. Such a resonant nature of the Raman intensity is best observed by a tunable laser in which the intensity is enhanced in a factor of 1000 within a small laser energy range of about 20 meV.[9] Since the van Hove singular energy positions E_{ii} depend in a unique way on the diameter and chirality of each (n, m) nanotube,[10,11] the probability of finding a resonant tube in a laser spot of 1 μm diameter is about 1/100–1/10 when the nanotube density is 1–10 per 1 μm^2, respectively, for typical samples of isolated SWNTs that have been prepared having a diameter distribution of $d_t = 1.85 \pm 0.65$ nm.[5]

Even though there are often more than two nanotubes within a laser spot, it is rare that both tubes are resonant and thus yield two different Raman spectra. Therefore it is convenient to observe the Raman spectra from one nanotube by using a sample with several nanotubes per 1 μm^2. However, when we want to carry out a detailed study of different SWNT phonon modes, we need to use a low density sample (less than 1 nanotube per μm^2). In first-order Raman processes, there are two resonant conditions: (1) resonance with incident photon and (2) resonance with the scattered photon, in which the E_{ii} matches E_{laser} and $E_{\text{laser}} - E_{\text{phonon}}$, respectively. When we observe different resonant Raman modes from a nanotube, the resonant condition should be with the incident photon, since the phonon energy ($\sim$0.1 eV for optical phonon modes) is much larger than the resonant window (20 meV, as mentioned above). In the actual experiments, we used a low density sample in which the number of nanotubes per laser spot is less than unity to exclude the possibility that two peaks in the observed spectra come from different nanotubes with different resonant conditions. Although it takes a lot of time to get spectra for a low density sample, we have collected many spectra, especially for the case that both the RBM and G-band phonon modes are observed as a resonance with the incident photon.[7,12,13]

2. Assignment of (n, m) by Raman Spectra

There are several different Raman approaches that can be used to assign (n, m) to a single nanotube. An internal check using different approaches then can be used to confirm the assignment. In this section, we overview three results obtained from the first-order RBM and G-band Raman modes.

2.1 Diameter dependence of the RBM frequency

The RBM frequency does not depend on the chirality but only on the diameter and is inversely proportional to the diameter for a wide range of diameters, d_t, from 1 to 2 nm.[14] The phonon frequency is expressed by $\omega_{\mathrm{RBM}} = \alpha/d_t$, where α is constant with values ranging from 234[15] to 248 $\mathrm{cm}^{-1}\mathrm{nm}$.[5] First principles calculations[16,17] also give similar values. As a first approximation, the van Hove singularity energies E_{ii} are inversely proportional to the diameter: for example $E_{11}^S = 2\gamma_0 a_{C-C}/d_t$ and $E_{11}^M = 6\gamma_0 a_{C-C}/d_t$ for the lowest E_{ii} for semiconducting and metallic SWNTs, respectively, (see Fig. 1) in which $\gamma_0 = 2.89\,\mathrm{eV}$ and $a_{C-C} = 1.44\,\text{Å}$ are, respectively, the tight-binding parameter and nearest neighbor carbon-carbon distance.[11] Thus, for a given laser energy E_{laser} and observed ω_{RBM}, we can determine d_t and select the best resonant E_{ii} value. The number of (n, m) nanotubes which satisfy both the d_t and E_{ii} values experimentally for a given ω_{RBM} are only one or two, if the accuracy of α is within the order of $1\,\mathrm{cm}^{-1}\mathrm{nm}$. The empirical value of α is chosen to satisfy observations on many different RBM peaks at the same time. Once the α and γ_0 are specified by $248\,\mathrm{cm}^{-1}\mathrm{nm}$ and 2.89 eV, respectively, for the conditions of our experiments, the assignment for (n, m) values is almost unique.[5] This set of parameters are independently obtained by Yu and Brus[18] to reproduce the Raman spectra obtained with their thin SWNT bundle sample.

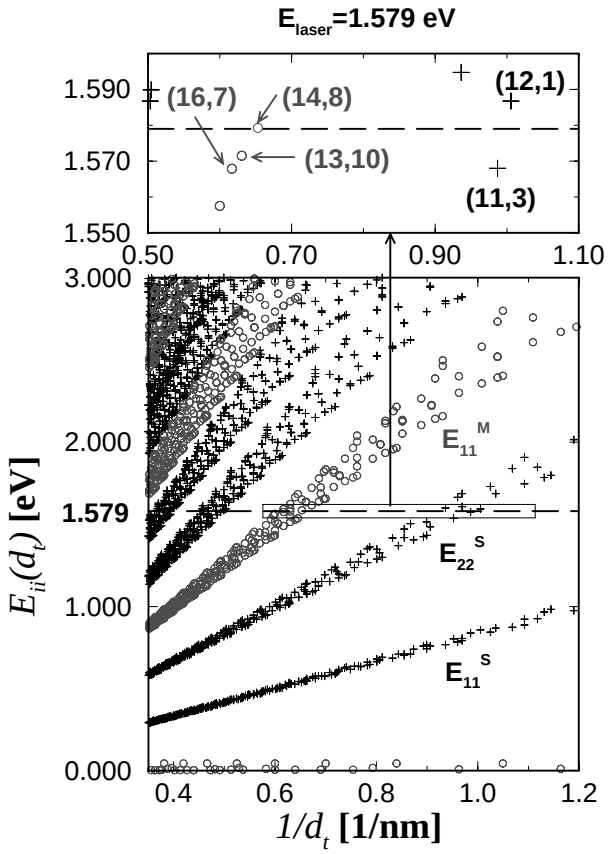

Fig. 1. Van Hove singular energy in JDOS, E_{ii} as a function of $1/d_t$ (the bottom figure) in which circles and cross correspond, respectively, to metallic and semiconducting chirality (n, m). For a 1.579 eV laser, expanding a rectangle section is shown in the upper figure. The (14,8) nanotube corresponds to rigorous resonance and the other nanotubes correspoind to pre-resonance situations.

2.2 Stokes and anti-stokes intensity ratio of the RBM

The resonant conditions for the Stokes and anti-Stokes processes are the same for the incident resonance condition $E_{ii} = E_{\mathrm{laser}}$, but different from each other for the scattered resonance condition $E_{ii} = E_{\mathrm{laser}} \pm E_{\mathrm{phonon}}$, where $\pm$ denotes the phonon emission (Stokes, $-$) and absorption (anti-Stokes, $+$) spectra, respectively. A typical phonon energy for the RBM phonon modes ($150\,\mathrm{cm}^{-1}$) is 18 meV, which is comparable to the rigorous-resonance window, 20 meV, as discussed above.[9] Under non-resonant conditions, the intensity ratio of the anti-Stokes to Stokes intensities is given by the Boltzmann factor, $\exp(-E_{\mathrm{phonon}}/k_{\mathrm{B}}T)$, but this is not the case for the resonance Raman process in which the relative integrated intensity I_{AS}/I_S is governed by the resonant condition. In fact for some cases, the normalized anti-Stokes peak gives a larger intensity than the Stokes peak. Using this fact, we can clearly distinguish between (n, m) values for tubes which accidentally give the same diameter and thus the same phonon frequency. Even though two (n, m) values give the same phonon frequency, the E_{ii}'s do not have the same value, and this is because of the effect of trigonal warping on the electronic energy band structure which results in chirality-dependent E_{ii} values.[11] The special case where two SWNTs have ω_{RBM} values within $1\,\mathrm{cm}^{-1}$ does not occur frequently, thus providing evidence that our selection of the two parameters α and γ_0 allows us to predict the E_{ii} reliably from the measured Stokes to anti-Stokes intensity ratio, without any exception.

2.3 Chirality dependent G-band intensity

The E_{2g} Raman-active mode of 2D graphite, appearing at $1582\,\mathrm{cm}^{-1}$ as an isotropic in-plane doubly degenerate mode, is split in SWNTs by the cylindrical tubular shape and the curvature effect.[19] Because of symmetry lowering in SWNTs, six phonon modes [$2A + 2E_1 + 2E_2$ modes denoted as longitudinal and transverse optic (LO and TO) phonon modes] can be generally Raman active for chiral nanotubes. For achiral nanotubes, such as armchair and zigzag nanotubes, which have mirror symmetry parallel to the nanotube axis, only three of the six symmetry modes (A_{1g}, E_{1g} and E_{2g}) are Raman-active. These two results should connect smoothly as a function of chiral angle that defines the spiral structure of SWNTs. The bond-polarization theory predicts that the relative Raman intensity for each symmetry has a chiral angle dependence, which smoothly connects in the actual experiments to the cases of achiral nanotubes.[8] In experiments, however, we need to also consider the strong depolarization effect, whereby a photon is preferentially absorbed when the polarization vector is parallel to the nanotube axis.[20] Nevertheless, experimentally, the G-band is split into two major peaks (G^+ and G^-) whose relative intensities depend on the chiral angle of the nanotube. The (n, m) values, tentatively assigned by analysis of the RBM feature, predict the chirality dependence of the relative intensities of the G^+ and G^- band.[18,20]

3. Second-Order Raman Spectra

The assignment of (n, m) can be confirmed, too, by measuring diameter and chirality dependent effects on the disorder-induced D-band and its second harmonic G′-band. The D-band and G′-band features are observed in a second-order Raman process by which two scattering processes occur. Here we start with the background of second-order Raman processes.

3.1 D-band and G′-band of graphite

The D-band is observed in many graphitic materials at around $1355\,\mathrm{cm}^{-1}$ for a laser excitation energy $E_{\mathrm{laser}} = 2.41\,\mathrm{eV}$,[1,16,21–23] and the G′-band which is the second harmonic of the D-band, appears at about $2710\,\mathrm{cm}^{-1}$. The D-band and G′-band features are explained by a second-order Raman scattering process and by double resonance theory.[23] Second-order Raman spectra are generally weak and broad when compared with first-order Raman processes. However, if two of the three intermediate states for an excited electron-hole pair, known as an exciton, are real electronic states, resonance enhancement occurs twice, and thus the corresponding Raman intensity might be comparable to that of a first-order process.[24] Such an effect is known as a double resonance Raman process.[25] An important fact in the second-order process is that the scattering q vectors are not always zero, because a pair of q and $-q$ scattering wave vectors can often make a round trip back to the original excited electron k states to recombine with the hole. Thus non-zone-center phonon modes are related to the D-band and G′-band features. For the D-band spectra, which is a one-phonon process, one of the two processes is an elastic electron scattering event, induced by the defect. The D-band intensity can be even stronger than the G-band intensity for a highly disordered carbon material.[26,27] On the other hand, in the case of the G′-band, both q and $-q$ vectors can be inelastic processes, and thus no defect is needed. In most graphitic materials, the G′-band is much stronger than the D-band, and the G′-band feature does not depend sensitively on the amount of disorder.

Another important factor about two-dimensional (2D) graphite, is that the initial electron and hole k vectors are around the K point [the corners of the hexagonal Brillouin zone (BZ)] where the bonding and anti-bonding π bands touch each other. Because the two carbon atoms in the unit cell are not equivalent, the bonding and anti-bonding electronic bands show a linear k dispersion relation, $E(k) = \sqrt{3}\gamma_0 ka/2$ in which the electronic k vectors are measured from the K point, and $a = \sqrt{3}a_{C-C} = 2.46\,\text{Å}$. Thus when E_{laser} increases, the electron k vectors and the corresponding phonon q vectors both increase, giving rise to a dispersion of the D-band phonon frequency which increases by $53\,\mathrm{cm}^{-1}/\mathrm{eV}$ ($106\,\mathrm{cm}^{-1}/\mathrm{eV}$ for G′-band) for E_{laser} in the visible range. It is noted that the scattering q vectors are taken from one K point to an inequivalent K′ point (inter-valley scattering),[16,23,28] since the D-band phonon frequency is related to the phonon dispersion relation around the K point in 2D graphite. If the q vectors are given by intra-valley scattering from K to K (or from K′ to K′), the non-zone-center phonon mode around the Γ point is relevant to the second-order, double-resonance phonon mode.[28] The corresponding Raman spectra can explain dispersive phonon modes appearing in the lower energy region of the spectra for a graphite whisker,[29] which is assigned to the acoustic phonon dispersion branch. Using the relation $q = 2k$ which comes from the singularity in the density of q vectors, most of the observed dispersive weak phonon modes are explained by either intra-valley or inter-valley phonon modes.[28]

Before concluding this subsection, let us list unsolved observations in graphite that can be explained by the double resonance effect: (1) disorder-induced phonon modes are dispersive, (2) Stokes and anti-Stokes phonon frequencies are slightly different from each other, (3) the G′-band phonon frequency $\omega_{G'}$ is not exactly equal to twice ω_D, and (4) many weak features of the dispersive Raman modes are explained as non-zone-center phonon modes in the phonon dispersion relations. There is now overwhelming evidence that the double resonance theory is generally relevant to the dispersive Raman modes.[28]

3.2 D-band and G′-band of SWNTs

In the case of SWNTs, the 2D electronic and phonon energy dispersion relations of graphite are zone-folded along the circumferential direction, which is realized by cutting the 2D BZ by lines, to obtain a set of 1D energy dispersion relations for SWNTs. The double resonance theory of graphite can be applied to SWNTs based on the zone-folded BZ or on cutting lines in the extended 2D BZ. For simplicity, we explain the double resonance in the non-zone-folded 2D BZ. As is discussed in the previous section, van Hove singularities in the JDOS are essential for obtaining Raman spectra from a single nanotube. Each van Hove singularity in the JDOS comes from the flat energy dispersion point on the cutting line, denoted by k_{ii}.[30] When the initial (final) k and (or) the scattered $k+q$ are van Hove singular k_{ii} points, the corresponding D-band and G′-band features are enhanced significantly.

In the case of the G′-band of SWNTs, it is not generally possible that both k and $k + q$ are simultaneously k_{ii} points, since the $E(k)$ and $E(k + q)$ states have different phonon energies. Thus, even if the double resonance condition were satisfied for the 1D k and $k + q$ vectors, either $E(k)$ or $E(k+q)$ would not correspond to a van Hove singular energy. An anomalous special situation might occur when the energy difference between two different E_{ii}'s of a SWNT coincides with the phonon energy. This situation is possible for special metallic nanotubes, for which the DOS is split into two peaks by the trigonal warping effect[30] and the splitting happens to equal a phonon frequency.

In the case of the D-band of SWNTs, it is possible that both the k and $k + q$ wavevectors are k_{ii} points, since the initial k and final $k+q$ states can have the same energy if the scattering process is elastic. In general there are four possible, second-order, one-phonon emission, double resonance processes. The factor of four comes from resonance with either the incident or scattered photon and from either the elastic or the inelastic scattering event occurring first in the sequence of the two consecutive processes. The corresponding phonon q vectors give two different phonon frequencies, depending only on whether the elastic or the inelastic scattering process occurs first.[31,32] In PPP-derived disordered graphite, the D-band spectra can be fitted to two Lorentzian lines which have about the same intensity, showing the same probability for getting each q vector. In the case of SWNTs, even though two of the four cases,

for which both the initial and final states of the elastic process are real electronic states, has a significant Raman intensity at the van Hove singularity as mentioned above, these two processes give different phonon frequencies, and thus the observed D-band spectra of the SWNT should be fit by two Lorentzians.

In the experiment, we observe the D-band spectra for an isolated single wall carbon nanotube when an optical transition occurs between VHSs from the valence to the conduction bands.[33] The resonant nature of a given D-band spectrum has not yet been observed by a tunable laser but we can explain the oscillatory behavior of the D-band and G′ band observed in SWNT bundles[34] by the double resonance process.[16,30,33] When an equi-energy contour touches the cutting lines of the 1D BZ, the touching point corresponds to k_{ii}. The double resonance process occurs from or to k_{ii} points in the case of SWNTs, while all k points on the energy contour are possible for 2D graphite. The overall contribution to the Raman intensity not only for the rigorous resonance condition but also for the pre-resonance condition from many k points should be calculated by integrating for all processes, and such a calculation will be reported elsewhere.[32] In fact, the line width of the D-band of a SWNT is much smaller ($10\,\mathrm{cm}^{-1}$) than that for graphite ($\sim 50\,\mathrm{cm}^{-1}$). The distance of this k_{ii} point from the K point of the BZ determines the resonant energy E_{ii} and the phonon frequency ω_D. Since the direction of the cutting lines depends on the chiral angle,[19] the chirality dependence of ω_D for isolated SWNTs is well explained by the distance of the k_{ii} points from the K point.[33] The inter-valley phonon q vectors which connect two k_{ii} points A and B are shown in Fig. 2. When A is located at k_{ii}, the inequivalent B point is located at $-k_{ii}$, and for any position of k_{ii}, we can shift A and B to the nearest K and K′ points as shown in Fig. 2, using the periodicity of k in BZ. Further when we shift the A point to the Γ point, the final point B moves to C which lies at a $-2k_{ii}$ position from the same K′ point. Thus, the phonon frequency of the D-band is relevant to the k_{ii} distance, and more precisely to the opposite side of k_{ii} for the K point. Since the trigonal warping effect affects both the k_{ii} position and the phonon frequency, a chirality dependence of the D-band frequency is observed.[33]

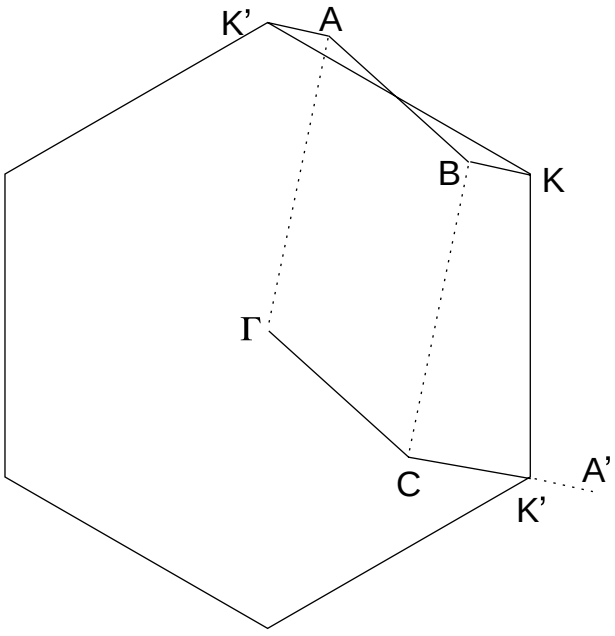

Fig. 2. Second-order scattering q vector for a single wall carbon nanotube. A and B are the van Hove singular k_{ii} points and the vector AB corresponds to the phonon wavevector. When we move the vector AB to ΓC, it is clear that $\mathrm{K'C} = 2\mathrm{K'A'}$ in which A′ is equivalent to the A point in the 2D Brillouin zone.

Thus the D-band and G′-band frequencies as a function of (n, m) can provide another example for checking the internal consistency of the (n, m) assignment.

4. Summary

In summary, micro Raman spectroscopy makes it possible to assign (n, m) values from a single Raman spectrum. The (n, m) assignment can then be confirmed by determination of the: (1) RBM resonance condition and the chirality dependent E_{ii}, (2) Stokes and anti-Stokes intensity ratio of the RBM, (3) chirality dependent relative intensities of the splitting of the G-band spectra, and (4) chirality dependent D-band and G′-band phonon frequencies. A more rapid and precise (n, m) determination should be made by a tunable laser covering a much larger laser energy range. Then the overall spectra from the incident and scattered light resonances of many different features of the Raman spectra will be obtained, in much better detail. This will be the subject of a future study.

Acknowledgements

The authors thank many collaborators for doing the experiments related to this subject and for sharing their results with us. R.S. acknowledges UFMG for supporting the visit to UFMG on this subject and a Grant-in-Aid (No. 13440091) from the Ministry of Education, Science, Japan. M.A.P. acknowledges NSF-CNPq joint collaboration grant (CNPq #910120/99-4). A.J./A.G.S.F. acknowledge support from the Brazilian agency CNPq. The MIT authors acknowledge support under NSF Grants DMR 01-16042, INT 98-15744, and INT 00-00408.

1) M. S. Dresselhaus, G. Dresselhaus, A. Jorio, A. G. Souza Filho and R. Saito: to be published in Carbon (2002).
2) M. S. Dresselhaus, A. Jorio, A. G. Souza Filho, G. Dresselhaus and R. Saito: to be published in Physica B (2002).
3) M. S. Dresselhaus, A. Jorio, A. G. Souza Filho, G. Dresselhaus, R. Saito and M. A. Pimenta: to be published in Liq. Cryst. Mol. Cryst. (2002).
4) M. S. Dresselhaus, G. Dresselhaus, A. Jorio, A. G. Souza Filho and R. Saito: to be published in Accounts of Chemical Research (2002).
5) A. Jorio, R. Saito, J. H. Hafner, C. M. Lieber, M. Hunter, T. McClure, G. Dresselhaus and M. S. Dresselhaus: Phys. Rev. Lett. **86** (2001) 1118.
6) A. G. Souza Filho, A. Jorio, J. H. Hafner, C. M. Lieber, R. Saito, M. A. Pimenta, G. Dresselhaus and M. S. Dresselhaus: Phys. Rev. B **63** (2001) 241404R.
7) A. G. Souza Filho, A. Jorio, G. Dresselhaus, M. S. Dresselhaus, Anna K. Swan, M. S. Ünlü, B. B. Goldberg, R. Saito, J. H. Hafner, C. M. Lieber and M. A. Pimenta: Phys. Rev. B **65** (2002) 085417.
8) R. Saito, A. Jorio, J. H. Hafner, C. M. Lieber, M. Hunter, T. McClure, G. Dresselhaus and M. S. Dresselhaus: Phys. Rev. B **64** (2001) 085312.
9) A. Jorio, A. G. Souza Filho, G. Dresselhaus, M. S. Dresselhaus, R. Saito, J. H. Hafner, C. M. Lieber, F. M. Matinaga, M. S. S. Dantas and M. A. Pimenta: Phys. Rev. B **63** (2001) 245416.
10) H. Kataura, Y. Kumazawa, Y. Maniwa, I. Umezu, S. Suzuki, Y. Ohtsuka and Y. Achiba: Synthetic Metals **103** (1999) 2555.
11) R. Saito, G. Dresselhaus and M. S. Dresselhaus: Phys. Rev. B **61** (2000) 2981.

12) M. A. Pimenta, A. Jorio, S. D. M. Brown, A. G. Souza Filho, G. Dresselhaus, J. H. Hafner, C. M. Lieber, R. Saito and M. S. Dresselhaus: Phys. Rev. B **64** (2001) 041401.
13) A. Jorio, A. G. Souza Filho, G. Dresselhaus, M. S. Dresselhaus, A. K. Swan, B. Goldberg, M. S. Ünlü, M. A. Pimenta, J. H. Hafner, C. M. Lieber and R. Saito: Phys. Rev. B **65** (2002) 155412.
14) R. Saito, T. Takeya, T. Kimura, G. Dresselhaus and M. S. Dresselhaus: Phys. Rev. B **57** (1998) 4145.
15) S. Bandow, S. Asaka, Y. Saito, A. M. Rao, L. Grigorian, E. Richter and P. C. Eklund: Phys. Rev. Lett. **80** (1998) 3779.
16) J. Kürti, V. Zólyomi, A. Grüneis and H. Kuzmany: unpublished.
17) D. Sanchez-Portal, E. Artacho, J. M. Soler, A. Rubio and P. Ordejón: Phys. Rev. B **59** (1999) 12678.
18) Z. Yu and L. E. Brus: J. Phys. Chem. B **105** (2001) 1123.
19) R. Saito, G. Dresselhaus and M. S. Dresselhaus: *Physical Properties of Carbon Nanotubes* (Imperial College Press, London, 1998).
20) A. Jorio, A. G. Souza Filho, V. W. Brar, A. K. Swann, M. S. Ünlü, B. B. Goldberg, A. Righi, J. H. Hafner, C. M. Lieber, R. Saito, G. Dresselhaus and M. S. Dresselhaus: Phys. Rev. B**65** (2002) 121402(R).
21) F. Tuinstra and J. L. Koenig: J. Chem. Phys. **53** (1970) 1126.
22) M. S. Dresselhaus and P. C. Eklund: Adv. Phys. **49** (2000) 705.
23) C. Thomsen and S. Reich: Phys. Rev. Lett. **85** (2000) 5214.
24) R. M. Martin and L. M. Falicov: *Light-Scattering in Solids*, ed. M. Cardona, (Springer-Verlag, Berlin, 1975) p. 80.
25) M. Cardona: *Light-Scattering in Solids*, eds. M. Cardona and G. Güntherodt (Springer-Verlag, Berlin, 1982) p. 19.
26) M. S. Dresselhaus and R. Kalish: *Ion Implantation in Diamond, Graphite and Related Materials* (Springer-Verlag, Berlin, 1992) Springer Series in Materials Science.
27) A. C. Ferrari and J. Robertson: Phys. Rev. B **64** (2001) 075414.
28) R. Saito, A. Jorio, A. G. Souza Filho, G. Dresselhaus, M. S. Dresselhaus and M. A. Pimenta: Phys. Rev. Lett. **88** (2002) 027401.
29) P. H. Tan, C. Y. Hu, J. Dong, W. C. Shen and B. F. Zhang: Phys. Rev. B **64** (2001) 214301.
30) A. G. Souza Filho, A. Jorio, Ge. G. Samsonidze, G. Dresselhaus, M. S. Dresselhaus, A. K. Swan, B. B. Goldberg, M. S. Ünlü, R. Saito, J. H. Hafner, C. M. Lieber and M. A. Pimenta: Chem. Phys. Lett. **354** (2001) 62.
31) L. G. Cançado, M. A. Pimenta, R. Saito, A. Jorio, L. O. Ladeira, A. Gueneis, A. G. Souza Filho, G. Dresselhaus and M. S. Dresselhaus: to be published in Phys. Rev. B (2002).
32) A. Grüneis, R. Saito, T. Kimura, L. G. Cançado, M. A. Pimenta, A. Jorio, A. G. Souza Filho, G. Dresselhaus and M. S. Dresselhaus: Phys. Rev. B **65** (2002) 155405.
33) A. G. Souza Filho, A. Jorio, G. Dresselhaus, M. S. Dresselhaus, R. Saito, A. K. Swan, M. S. Ünlü, B. B. Goldberg, J. H. Hafner, C. M. Lieber and M. A. Pimenta: Phys. Rev. B **65** (2002) 035404.
34) M. A. Pimenta, E. B. Hanlon, A. Marucci, P. Corio, S. D. M. Brown, S. A. Empedocles, M. G. Bawendi, G. Dresselhaus and M. S. Dresselhaus: Brazilian J. Phys. **30** (2000) 423.